

Southern Ocean mixed-layer depth from Argo float profiles

Shenfu Dong,¹ Janet Sprintall,² Sarah T. Gille,² and Lynne Talley²

Received 9 December 2006; revised 28 November 2007; accepted 26 February 2008; published 13 June 2008.

[1] Argo float profiles of temperature, salinity, and pressure are used to derive the mixed-layer depth (MLD) in the Southern Ocean. MLD is determined from individual profiles using both potential density and potential temperature criteria, and a monthly climatology is derived from individual MLDs using an objective mapping method.

Quantitative data are available in the auxiliary material. The spatial structures of MLDs are similar in each month, with deep mixed layers within and just north of the Antarctic Circumpolar Current (ACC) in the Pacific and Indian oceans. The deepest mixed layers are found from June to October and are located just north of the ACC where Antarctic Intermediate Water (AAIW) and Subantarctic Mode Water (SAMW) are formed.

Examination of individual MLDs indicates that deep mixed layers ($MLD \geq 400$ m) from both the density and temperature criteria are concentrated in a narrow surface density band which is within the density range of SAMW. The surface salinity for these deep mixed layers associated with the SAMW formation are slightly fresher compared to historical estimates. Differences in air-sea heat exchanges, wind stress, and wind stress curl in the Pacific and Indian oceans suggest that the mode water formation in each ocean basin may be preconditioned by different processes. Wind mixing and Ekman transport of cold water from the south may assist the SAMW formation in the Indian Ocean. In the eastern Pacific, the formation of mode water is potentially preconditioned by the relative strong cooling and weak stratification from upwelling.

Citation: Dong, S., J. Sprintall, S. T. Gille, and L. Talley (2008), Southern Ocean mixed-layer depth from Argo float profiles, *J. Geophys. Res.*, 113, C06013, doi:10.1029/2006JC004051.

1. Introduction

[2] The ocean mixed layer is characterized as having nearly uniform physical properties throughout the layer with a gradient in properties at the bottom of the layer. The mixed layer links the atmosphere to the deep ocean and plays a critical role in climate variability. Atmospheric fluxes of momentum, heat and freshwater through the ocean surface drive vertical mixing that generates the mixed layer. The depth of the mixed layer varies with time owing to variability of the atmospheric forcing, and the thickness of the mixed layer indicates the amount of water (as well as heat) that directly interacts with the atmosphere.

[3] A recent mixed-layer heat balance analysis in the Southern Ocean [Dong et al., 2007] suggests that a proper representation of the temporal variations of mixed-layer depth (MLD) is required in order to obtain a more accurate upper ocean thermal balance involving the air-sea heat exchange. The heat stored and released from the ocean involves subduction/obduction processes (water leaving or entering the mixed layer from the layer below) that depend on the temporal and spatial variability of the MLD.

Dommenget and Latif [2002] suggested that the MLD strongly influences sea surface temperature (SST) variability and that a better representation of the MLD can improve the predictability of the SST anomalies on seasonal to longer timescales. The persistence of wintertime SST anomalies is related to the seasonal and interannual variability of the MLD through a reemergence mechanism [Alexander and Deser, 1995; Deser and Timlin, 2003]. Bhatt et al. [1998] suggested that the reemergence mechanism also acts to enhance the persistence of air temperature anomalies on interannual timescales through air-sea interaction. Thus, a better knowledge of the MLD can improve our understanding of the atmosphere-ocean coupled system.

[4] A proper representation of the mixed layer in the Southern Ocean is particularly important. The strong winds in the Southern Ocean imply deep mixing, and hence deep mixed layers. Deep mixed layers are linked to Antarctic Intermediate Water (AAIW) and Subantarctic Mode Water (SAMW) formation [McCartney, 1977; Hanawa and Talley, 2001]. The process of AAIW and SAMW formation connects the upper and lower limbs of the global overturning circulation [Sloyan and Rintoul, 2001], which carries heat around the globe. Properties of SAMW and AAIW contain the imprint of air-sea interaction and carry carbon dioxide into the ocean interior, resulting in a possibly large storage of anthropogenic carbon dioxide. SAMW in particular has been claimed as a good indicator of anthropogenic climate change [Banks et al., 2000, 2002].

¹CIMAS/RSMAS, University of Miami, Miami, Florida, USA.

²Scripps Institution of Oceanography, University of California, San Diego, La Jolla, California, USA.

[5] A number of global MLD products are publicly available [e.g., *Monterey and Levitus*, 1997; *de Boyer Montegut et al.*, 2004]. Examination of the mixed-layer heat budget in the Southern Ocean [*Dong et al.*, 2007] suggests that there are large uncertainties in the MLD from the World Ocean Atlas 1994 [*Monterey and Levitus*, 1997]. The MLD of *de Boyer Montegut et al.* [2004] provides a better representation of the mixed layer. However, their density-based MLD has large gaps in the Southern Ocean because of the sparseness of the historical salinity observations. Argo floats measure both temperature and salinity stratification, providing a unique data set for the Southern Ocean to determine MLD. The vertical resolution of the Argo float profiles is relatively coarse, which may not be suited for resolving shallow MLDs typical of the tropics. However, Argo float profiles have the potential to resolve the deeper MLDs commonly seen in the Southern Ocean. The main objective of this study is to determine a climatology for the Southern Ocean MLD from Argo float profiles. Keeping in mind the relationship between the deep mixed layers and the formation of AAIW and SAMW, we will also examine where and when the deep winter mixed layers occur and their water properties. Some recent studies [*Sallee et al.*, 2006; *Schneider and Bravo*, 2006; J. W. Holte and L. Talley, Examining SAMW formation with a new method for finding mixed layer depths and ARGO, submitted to *Journal of Atmospheric and Oceanic Technology*, 2008] have used Argo floats to look at regional SAMW properties in the Southern Ocean. In this study we consider SAMW properties in the entire Southern Ocean.

[6] We start in section 2 with a description of the Argo profiles and the criteria used to determine MLD. Our MLD climatology is available in the auxiliary material¹ (see Appendix A). In section 3 we examine the spatial distribution and properties of deep mixed layers which mainly occur near the northern boundary of the Antarctic Circumpolar Current (ACC). The temperature, salinity, and density of these deep mixed layers are consistent with the property ranges of the SAMW. A summary is given in section 4.

2. Data and Criteria for the Ocean Mixed-Layer Depth

[7] Argo float profiles of temperature, salinity and pressure [*Gould and the Argo steering team*, 2004] during the period July 2001 to September 2006 are used to compute MLD in the Southern Ocean (30°S – 65°S , 0°E – 360°E). Each float descends to a preprogrammed parking depth (typically 1000 to 2000 m) and drifts freely. Every 10 d it ascends from its parking depth to the sea surface. As it rises, temperature and salinity are measured continuously. When the float reaches the surface, the continuous measurements are averaged with 10 m resolution in the top 200 m of the water column, and below 200 m the average spacing increases linearly with depth to about 100 m at 2000 m depth. The averaged measurements are then transmitted to satellites. After transmission, the float descends again and starts a new cycle. Argo provides seasonally unbiased measurements, which are critical for climate studies, par-

ticularly at high latitudes where ship measurements are limited during winter owing to the hostile weather conditions. The global Argo profiles and trajectories are managed by the Global Ocean Data Assimilation Experiment and available from <http://www.usgoda.org/>. Only profiles with a quality flag of ‘1’ and ‘2’, indicating ‘good data’ and ‘probably ‘good data’, are used, resulting in a total of about 42,000 profiles in our study region. About 3% of those profiles extend to less than 200 m depth and are excluded to ensure the detection of the mixed layer. Another 1% of the profiles are also excluded because of density inversions. Although the number of profiles in each month does not differ significantly, the number has increased enormously each year with 88% of the total profiles obtained during 2004–2006.

[8] Here we describe the vertical structure of the temperature in the Southern Ocean and divide Argo profiles into 3 groups based on a common temperature structure and location: common stratification (Figure 1a), temperature inversion near the Polar Front (Figure 1b), and temperature inversion near the ACC (Figure 1c). Examples of typical temperature and salinity profiles for each group are shown in the middle and lower plots of Figure 1. Argo profiles, particularly north of the ACC (Figure 1a), are typically stratified, with increasing density (not shown) and decreasing temperature with depth (Figure 1a, middle). Here we define the ACC region as a circumpolar band between the mean dynamic heights of -0.4 m and -1.2 m , corresponding to the Subantarctic Front and Polar Front, respectively, where the mean dynamic heights are from *Maximenko and Niiler* [2005]. Those dynamic heights are similar to the mean positions of the Subantarctic Front and Polar Front from historical hydrographic data [*Orsi et al.*, 1995; *Belkin and Gordon*, 1996] and satellite measurements [*Gille*, 1999; *Moore et al.*, 1999; *Dong et al.*, 2006]. For most profiles salinity decreases with depth from the surface to about 1000 m, and below that it increases with depth (Figure 1a, bottom, solid line). In the eastern Pacific (east of 150°W) and in the vicinity of the ACC salinity increases with depth with the minimum salinity at the surface (Figure 1a, bottom, dashed line). This common thermally stabilized stratification makes up 76% of the total Argo profiles in our study region. The rest of the profiles experience temperature inversions because of the influence of salinity. Temperature inversions are common within and near the boundaries of the ACC, and they are frequently found in the Argo profiles (Figure 1b and 1c). Depending on the location and time of year, temperature inversions show different vertical structures.

[9] Nearly all the Argo profiles in the vicinity of the Polar Front and to its south experience temperature inversions (Figure 1b). These profiles typically have very weak stratification below 400–500 m depth, and the temperature at 1000 m is about 2°C , corresponding to the Upper Circumpolar Deep Water. Figure 1b (middle) illustrates the seasonal evolution of the temperature in the upper column. During winter (Figure 1b, middle, gray line), the minimum temperature at the surface extends to 100–300 m corresponding largely to the Antarctic Surface Water and Winter Water layers south of the Polar Front, whereas below 300 m, the water column is warmer, and the temperature gradient is weak. The upper layer warms in spring (Figure 1b, middle,

¹Auxiliary materials are available at <ftp://ftp.agu.org/apend/jc/2006jc004051>.

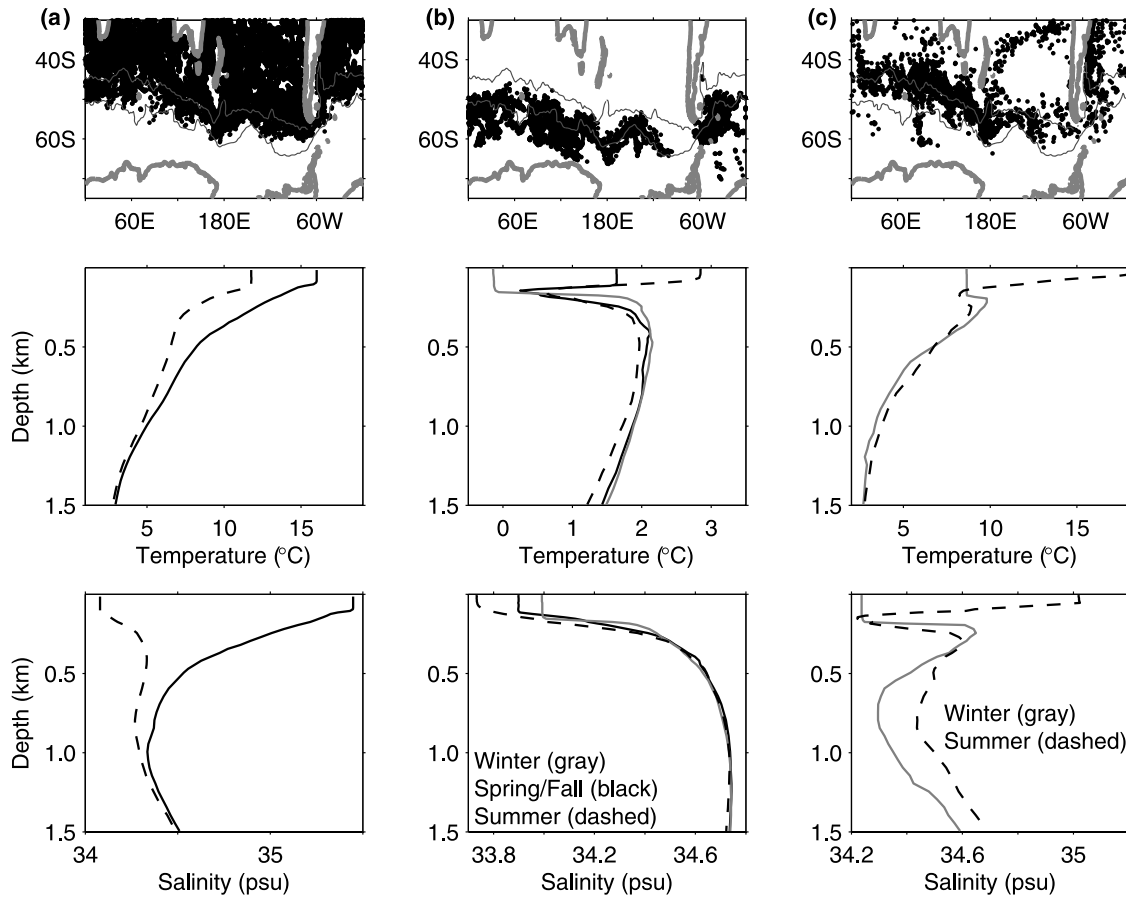


Figure 1. (top) Spatial distributions of Argo profiles with particular (middle) temperature and (bottom) salinity vertical structures: (a) the typical stratification of decreasing temperature with depth (middle), and examples of salinity (bottom) increasing (dashed, typical in the eastern Pacific and in the vicinity of the ACC) and decreasing (solid, typical in the western Pacific, Atlantic, and Indian oceans) with depth. (b, c) Profiles with temperature inversions but with different temperature structure in the upper water column. The black curves in the top plot are the mean SSH contours of -0.4 m (north) and -1.2 m (south), which are used to define the ACC.

black solid line), and the minimum temperature at 100–300 m is capped by warm water at the surface, but the surface temperature is still lower than the deeper water column. Summer heating further warms the upper water column, resulting in higher temperatures at the surface, which exceed the temperature maximum found at depth (Figure 1b, middle, dashed line). The surface temperature subsequently decreases as a result of cooling in fall, and profiles show a structure similar to that found in spring. The corresponding salinity profiles (Figure 1b, bottom) show that salinity decreases with depth during all seasons. A seasonal variation in salinity can be seen in the top 100–300 m layer with the freshest water during summer (Figure 1b, bottom, dashed line), which is probably due to the ice melting. Profiles shown in Figure 1b make up 12% of the total profiles.

[10] Temperature inversions are also common around the northern boundary of the ACC (Figure 1c), occur in the remaining 12% of the profiles. In contrast with temperature profiles to the south (Figure 1b), temperature profiles around the northern boundary of the ACC experience large stratification below the mixed layer, and the surface water is warmer than the deeper water column (Figure 1c, middle).

During winter, temperature profiles show a subsurface maximum (Figure 1c, middle, gray line). Similar to the seasonal evolution of the temperature inversion to the south (Figure 1b, middle), heat input from the atmosphere during summer warms the surface layer, which caps the cold water below the surface, and the temperature of the warmed surface layer exceeds the temperature maximum at the subsurface (Figure 1c, middle, dashed line). Temperature profiles during spring and fall (not shown) do not show a coherent vertical structure, and the surface temperature can be warmer or colder than the subsurface temperature. The vertical structure of the salinity profiles along the northern boundary of the ACC (Figure 1c, bottom) is more complicated than those in the other two cases (bottom plots in Figures 1a and 1b) owing to the mixing of water masses from the south and the north. Some salinity profiles show a vertical structure similar to those in Figure 1a, bottom, some show structure similar to those in Figure 1b, bottom, and others show multiple inversions as shown in Figure 1c, bottom.

[11] Overall, nearly one quarter of all our Argo profiles display temperature inversions (Figures 1b and 1c). These temperature inversions suggest that determination of the

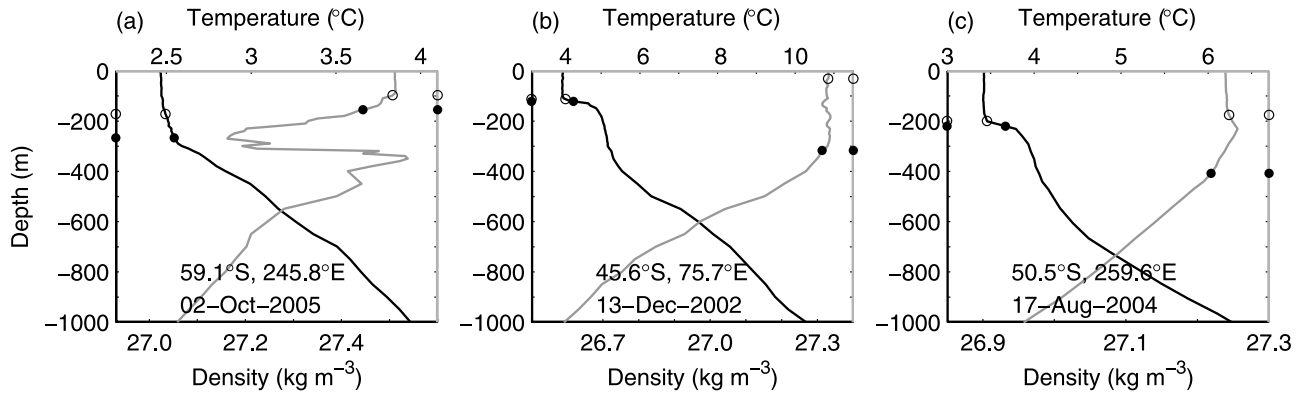


Figure 2. Examples of density (black lines) and temperature (gray lines) profiles from Argo floats where (a) the density profile has a deeper mixed layer than the temperature profile and (b, c) the temperature profile has a deeper mixed layer than the density profile. Dots and circles indicate the depth of mixed layer from the difference criteria and gradient criteria, respectively.

MLD in the Southern Ocean is likely to pose different challenges than determining MLDs in lower latitude regions that are strictly temperature stratified.

[12] A number of criteria have been used in the literature to define MLD from in situ observations of temperature and salinity profiles. These criteria can be divided into two groups: property difference-based criteria, where MLD is defined as the depth where the oceanic property has changed from a reference surface value by a constant amount [e.g., *de Boyer Montegut et al.*, 2004], and gradient-based criteria where MLD is defined as the depth where the vertical gradient of the property equals or exceeds a threshold value [e.g., *Lorbacher et al.*, 2006]. In the following we refer to these as difference criteria and gradient criteria, respectively. In temperature-based difference criteria, values of potential temperature absolute difference ($\Delta t = |T_s - T_d|$) ranging from 0.01°C to 1.0°C have been commonly used [*Weller and Plueddemann*, 1996; *Monterey and Levitus*, 1997; *Qiu*, 2000; *de Boyer Montegut et al.*, 2004], where T_s is near surface potential temperature and T_d is the potential temperature at depth. Values of potential density difference ($\Delta\rho = \rho_s - \rho_d$) from 0.005 kg m^{-3} to 0.125 kg m^{-3} have been used in the density-based difference criteria [*Brainerd and Gregg*, 1995; *Monterey and Levitus*, 1997; *de Boyer Montegut et al.*, 2004]. A temperature gradient of $0.025^\circ\text{C m}^{-1}$ and density gradient from 0.0005 kg m^{-4} to 0.05 kg m^{-4} have been used to determine MLD in the gradient criteria [*Brainerd and Gregg*, 1995; *Wijesekera and Gregg*, 1996]. *Lorbacher et al.* [2006] determined MLD on the basis of the shallowest extreme curvature of temperature profiles. Holte and Talley (submitted manuscript, 2008) developed a hybrid method to identify MLD constructed specifically for the Southern Ocean profiles within and north of the ACC; they showed that density criteria are relatively robust, but criteria based on temperature alone are inadequate in the presence of strong salinity stratification, as also shown here. Comparisons of MLD from difference and gradient criteria [*Brainerd and Gregg*, 1995; *Thomson and Fine*, 2003] have suggested that MLDs determined using a difference criterion are more stable.

[13] In analogy with *de Boyer Montegut et al.* [2004], we determine MLD from individual float profiles using two

methods. One is a net temperature difference criterion $|\Delta T| = 0.2^\circ\text{C}$ and the second is a density difference criteria $\Delta\rho = 0.03 \text{ kg m}^{-3}$, where the near surface (0 – 20 m) temperature and density are used as reference values. Over the region south of 30°S only 1.5% of the monthly climatological MLDs of *de Boyer Montegut et al.* [2004] are shallower than 20 m, whereas 10% of MLDs are shallower than 30 m, suggesting that 20 m is a sensible determination of “near surface.” In regions where the salinity effect on MLD is negligible (Figure 1a), the temperature and density criteria give similar MLDs. Although temperature inversions dominate the Argo profiles south of the ACC, in most cases the inversions do not influence the MLD: the density and temperature criteria produce MLDs that differ by less than 20 m in 82% of the profiles shown in Figure 1b. However, in some cases salinity effects can result in large differences between the density-based and temperature-based MLDs. Figure 2a shows a temperature profile with a shallow mixed layer (154 m), whereas the corresponding density profile shows a much deeper mixed layer (267 m) because of the compensation between temperature and salinity. Figure 2b shows an opposite case: temperature above 300 m varies very little, whereas density increases significantly at 100 m because of increasing salinity. The differences between the temperature-based and the density-based MLDs suggest that where studies require an estimate of the fully homogenized mixed layer at each grid point, the shallower of the two MLDs should be employed.

[14] We tested alternate net difference values of ΔT (0.5°C) and $\Delta\rho$ (0.125 kg m^{-3}), which both result in deeper mixed layers. We found that the deeper mixed layers increased the imbalance in our mixed-layer heat budget [Dong et al., 2007]. This suggests that criteria with large temperature and density differences are not appropriate in the Southern Ocean, where the stratification is relatively weak. Smaller net difference values of ΔT (0.1°C) and $\Delta\rho$ (0.01 kg m^{-3}) result in shallower mixed layers, but the differences from MLD based on ΔT (0.2°C) and $\Delta\rho$ (0.03 kg m^{-3}) are mostly within 20 m. Those smaller net difference values are more likely affected by anomalous spikes and small perturbations in the profiles. We also tested the gradient criteria [*Lorbacher et al.*, 2006]. Similar to the

smaller net difference values, in most cases the mixed-layer depth did not differ significantly from the depth found using the property difference criteria ($\Delta t = 0.2^\circ\text{C}$ and $\Delta\rho = 0.03 \text{ kg m}^{-3}$): MLD differences are less than 20 m in 84% of the total profiles. However, in cases where the profiles change slowly with depth and anomalous spikes may appear within the well-mixed layer (such as in Figure 2b), the gradient criteria can give an erroneously shallow MLD that can differ from the net difference criteria by more than 100 m. Consistent with previous studies [Brainerd and Gregg, 1995; Thomson and Fine, 2003], our examination suggests that the difference criteria give a more stable MLD. Finally, we tested the hybrid method of Holte and Talley (submitted manuscript, 2008), as a supporting exercise for their study. The density-based MLD from their hybrid method is similar to the MLD from density difference criteria, consistent with their regional results that a density difference criteria is adequate for characterizing the actual MLD. However, relatively large differences are found in their temperature-based MLDs and the MLDs from our temperature difference criterion (see auxiliary material for quantitative data).

[15] The presence of temperature inversions (Figures 1b and 1c) does not significantly influence the determination of MLD from temperature alone, provided that the absolute values of temperature difference are used in the MLD criterion (i.e., $\Delta t = |T_s - T_d|$). However, in studies of mixed-layer heat budgets, in addition to MLD, the temperature (T_d) of water entrained into the mixed layer from below is also needed to determine the entrainment term, which has been shown to play an important role in improving the heat budget, at least on seasonal timescales [Qiu, 2000; Vivier et al., 2002; Dong and Kelly, 2004; Dong et al., 2007]. The difference of the mixed-layer temperature and the temperature of entrained water, δT is used in computing the entrainment. A constant δT of 0.5°C or 1°C has been used in number of studies [e.g., Qiu, 2000]. However, the presence of temperature inversions implies that the mixed layer can actually warm by entraining warmer water from below, contradicting the traditional idea of cooling by entrainment. Dong et al. [2007] showed that a monthly climatological δT , defined as the difference between the temperature at the surface (T_s) and the temperature at the bottom of the mixed layer (T_d), is generally negative south of the ACC and in the Indian Ocean just north of the Subantarctic Front during the cooling season. Using a constant δT leads to a larger imbalance in the heat budget because of an incorrect representation for the entrainment [Dong et al., 2007]. Quantitative data for δT are available in the auxiliary material (see Appendix A).

3. Mixed-Layer Depth

3.1. Monthly Climatology of the Mixed-Layer Depth

[16] To create a monthly climatology, the individual MLDs determined using the density difference criterion are objectively mapped [Bretherton et al., 1976; Roemmich, 1983] using e-folding scales of 2 degrees in latitude, 5 degrees in longitude, and 30 d in time. These e-folding scales are derived from the autocorrelation of individual MLDs. The monthly MLDs (Figure 3; quantitative data are available in auxiliary material; see Appendix A) show

similar spatial structures in each month, with deep mixed layers within and just north of the ACC. Here the monthly mean dynamic heights of -0.4 m and -1.2 m define the ACC region, where the monthly mean SSH anomalies during 2002–2006 from satellite altimeter [Ducet et al., 2000] are added to the mean dynamic heights [Maximenko and Niiler, 2005]. The MLD experiences large seasonal variability with the deepest mixed layers in August/September (Figures 3h and 3i) and the shallowest mixed layers in January/February (Figures 3a and 3b). The deep mixed layers from June to October are generally located just north of the ACC (Figures 3f–3j). The deepest mixed layers in the Pacific and Indian oceans exceed 400 m. In contrast in the Atlantic the MLD is relatively shallow with a wintertime maximum of about 150 m. The deep mixed layer region to the north of the Subantarctic Front was first described by McCartney [1977]. It is consistent with the deep mixed layer region inferred from oxygen saturation [Talley, 1999; Hanawa and Talley, 2001] and is synonymous with the formation region of AAIW and SAMW.

[17] Salinity influences stratification in the Southern Ocean, as clearly demonstrated from the MLD differences between the density and temperature criteria (Figure 4). The differences in MLDs exceed 100 m to the north of the ACC during winter (Figures 4g–4j). In general, the density criterion gives a deeper mixed layer during the cooling season from July to October (Figures 4g–4j), particularly in the region from the eastern Indian Ocean to the Pacific where the maximum temperature in a large number profiles is found below the surface (Figure 1c). These deeper mixed layers from density are due to the compensation between temperature and salinity: the decrease in density associated with warmer temperatures is compensated by an increase in salinity. In contrast north of the Subantarctic Front in the eastern Pacific, MLDs from the temperature criterion are much deeper than those MLDs determined from the density profiles, as also shown by Holte and Talley (submitted manuscript, 2008). In this region, temperature profiles experience a weak temperature inversion (Figure 2c), but the subsurface temperature maximum is less than 0.2°C warmer than the surface temperature. Thus, this inversion cannot be detected by the temperature criterion of $|\Delta T| \geq 0.2^\circ\text{C}$, resulting in an apparently much deeper mixed layer. The temperature criterion also gives a much deeper mixed layer in a small region north of the ACC between 120°E and 140°E (Figures 4e–4j), where the temperature profiles show a structure similar to Figure 2c.

3.2. Relationship Between Deep Mixed Layers and SAMW

[18] Since the deep mixed layer region is synonymous with the formation region of AAIW and SAMW [McCartney, 1977; Talley, 1999; Hanawa and Talley, 2001], here we examine the profiles with deep mixed layers for the properties of SAMW. The temperature and salinity of SAMW vary with longitude as the ACC shifts southward [McCartney, 1977; Hanawa and Talley, 2001]. However, as first pointed out by McCartney [1977], the eastward decreasing temperature from the western Atlantic to the eastern Pacific is compensated by decreasing salinity, such that the eastward density increase of SAMW is weaker than if governed only by temperature. In agreement with McCartney [1977], the

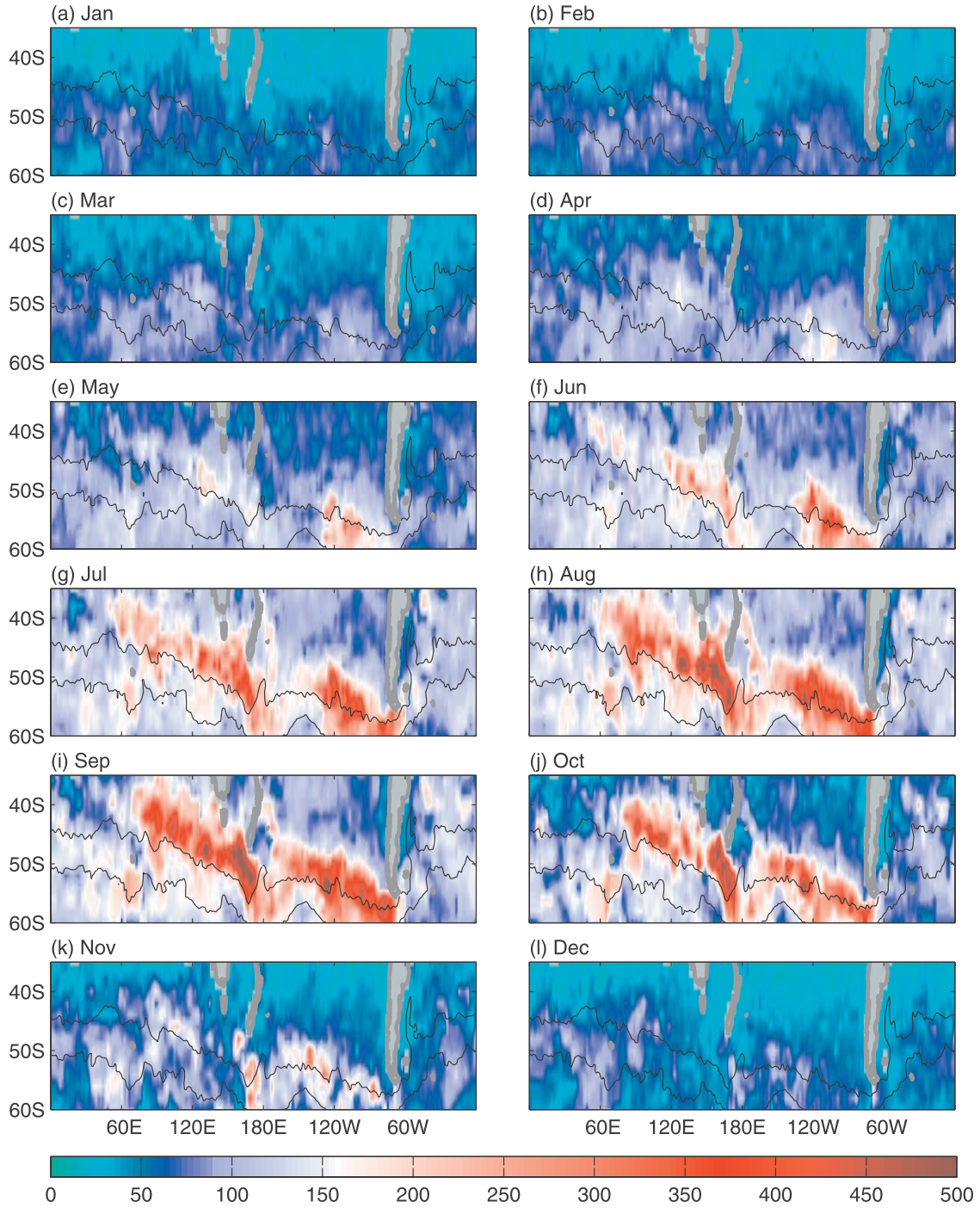


Figure 3. Objectively mapped monthly MLD (meters) from density criterion ($\Delta\rho = 0.03 \text{ kg m}^{-3}$) for (a) January through (l) December. The black curves are the monthly mean SSH contours of -0.4 m (north) and -1.2 m (south), which are used to define the ACC. Quantitative data are found in auxiliary material.

scatterplots of MLD against sea surface density (Figure 5) show that the deep mixed layers from both the density (Figure 5a) and temperature (Figure 5b) criteria are within a narrow density band. The surface density, temperature, and salinity for the profiles with MLD exceeding 400 m vary within the range of $26.57\text{--}27.04 \text{ kg m}^{-3}$, $4.3\text{--}13.3^\circ\text{C}$, and $34.1\text{--}35.3 \text{ psu}$, respectively. Both density and temperature are within the property range of the SAMW [Hanawa and

Talley, 2001]. However, the salinity of these deep mixed layers is slightly fresher than the salinity of historical measurements of SAMW ($34.2\text{--}35.8 \text{ psu}$) [Hanawa and Talley, 2001]. This might be explained by freshening observed in the intermediate waters of the North Pacific and Southern Ocean from six hydrographic sections from 1985 to 1994 during the World Ocean Circulation Experiment [Wong et al., 1999] compared to the historical data

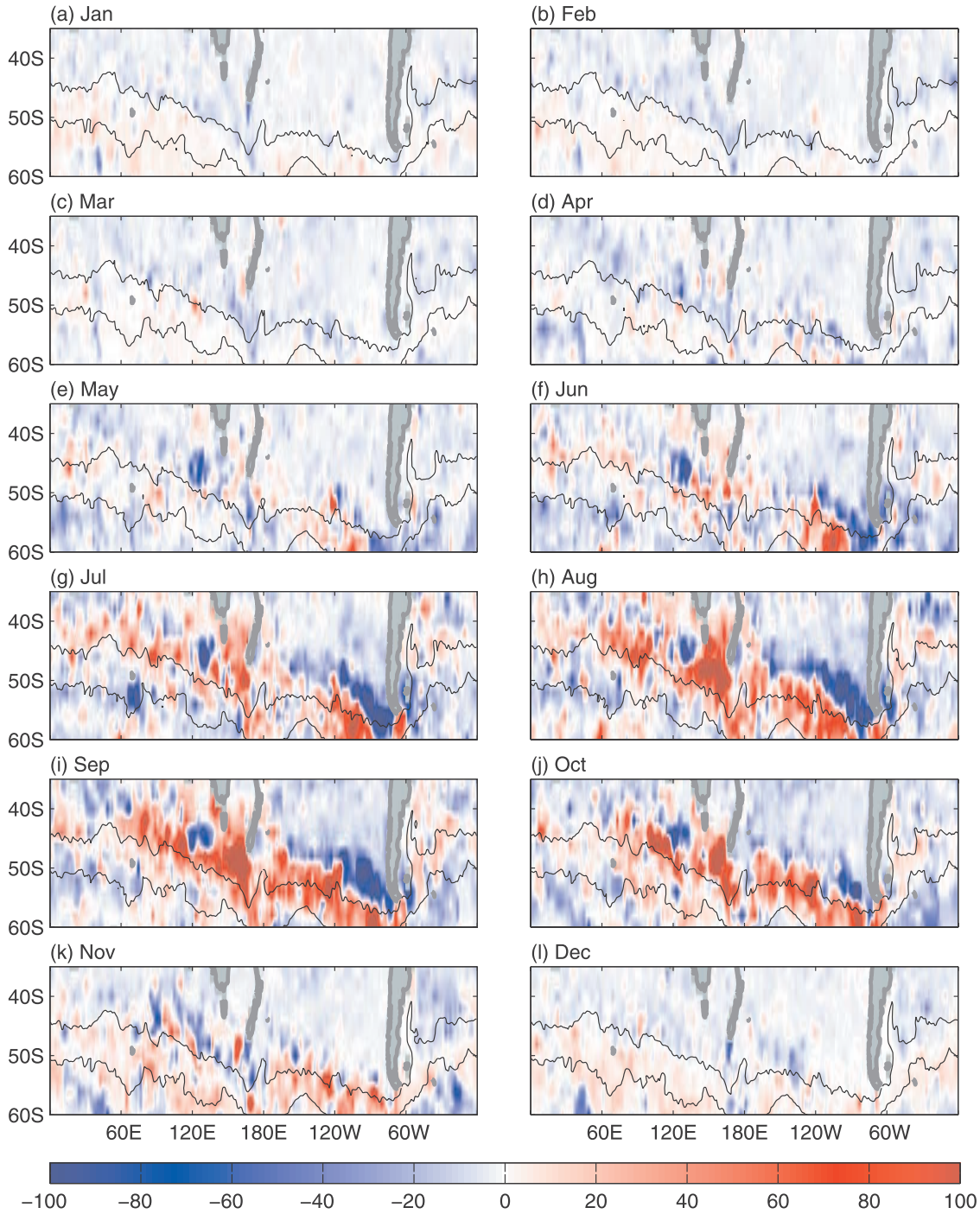


Figure 4. Differences in MLD (meters) using density ($\Delta\rho = 0.03 \text{ kg m}^{-3}$) and absolute value of temperature ($|\Delta T| = 0.2^\circ\text{C}$) difference criteria for (a) January through (l) December. Positive values (red) indicate that the density-based MLD is deeper than the temperature-based MLD. The black curves are the monthly mean SSH contours of -0.4 m (north) and -1.2 m (south), which are used to define the ACC. Quantitative data are found in auxiliary material.

collected between 1930 and 1980. Wong *et al.* [1999] attributed the freshening of the intermediate water to a salinity decrease of the surface waters due to an increase in precipitation over evaporation.

[19] Consistent with past observations of SAMW properties [Hanawa and Talley, 2001], the surface density and temperature for the deep mixed layers derived from the

Argo profiles vary spatially (Figure 6): density increases from 26.57 kg m^{-3} to 27.04 kg m^{-3} , and temperature decreases from 13.3°C to 4.3°C as the ACC shifts southward from the Indian Ocean to Drake Passage. As shown in Figure 6, these deeper mixed layers represent the thick SAMW found in the Indian and Pacific oceans. The deepest mixed layers ($\geq 600 \text{ m}$) are centered at 26.85 kg m^{-3}

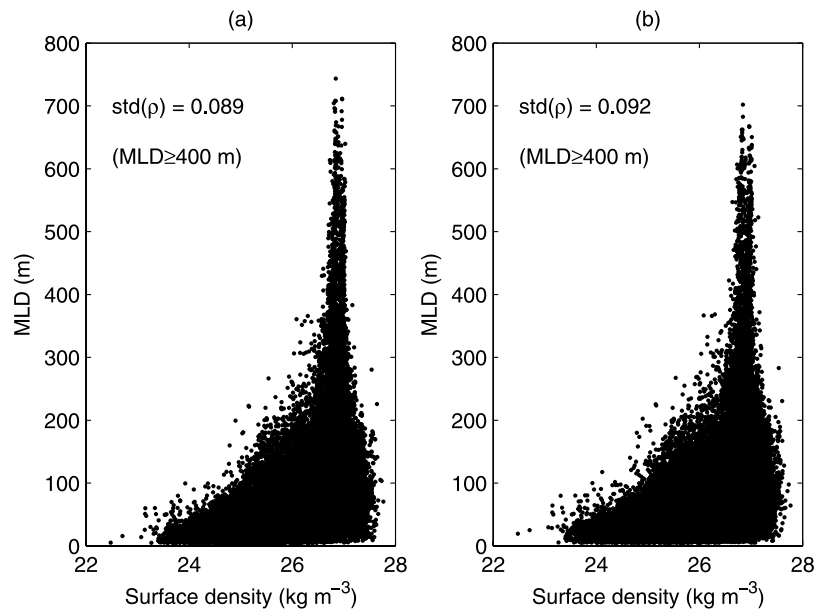


Figure 5. Scatterplots of MLD derived using (a) the density criterion and (b) the temperature criterion against near surface density from Argo float measurements.

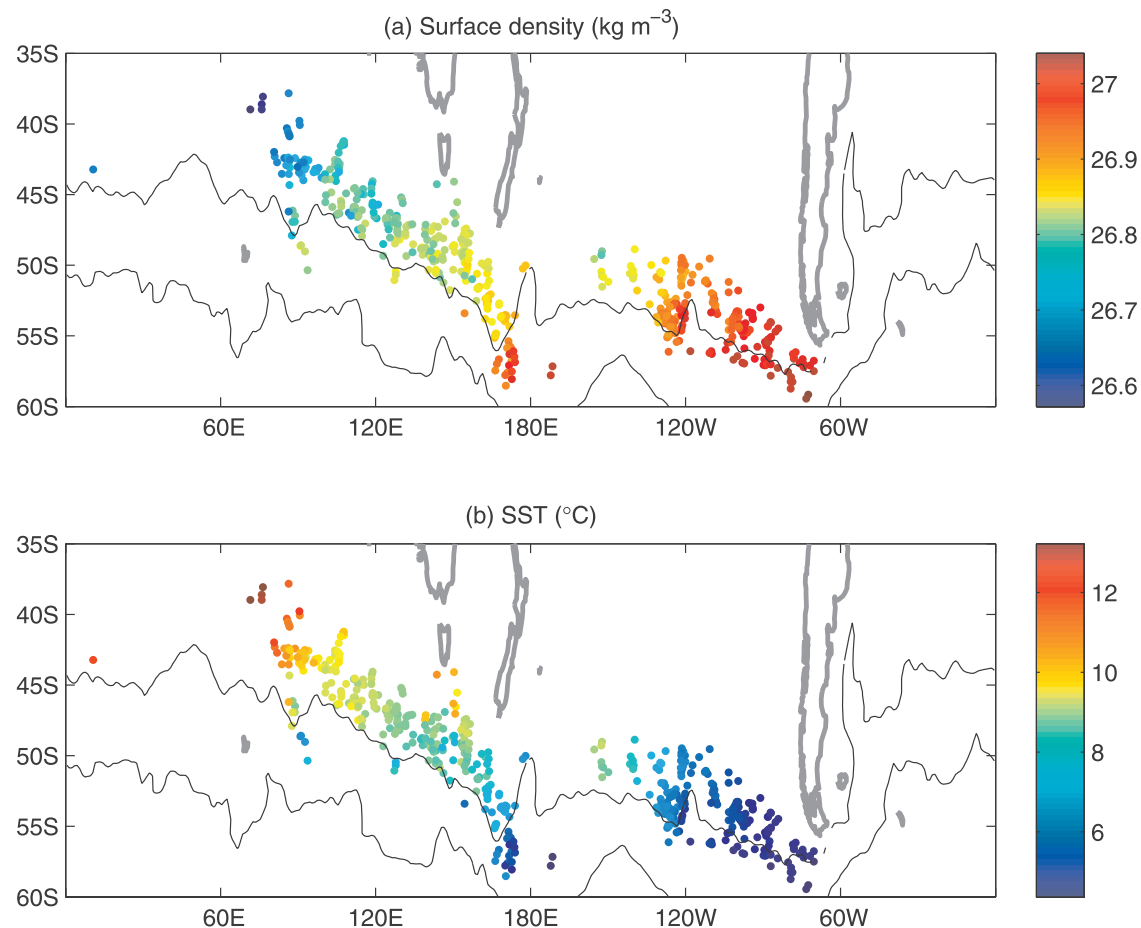


Figure 6. Spatial distribution of the near surface (a) density (kg m^{-3}) and (b) sea surface temperature ($^{\circ}\text{C}$) for MLDs that exceed 400 m. Black curves as in Figure 1.

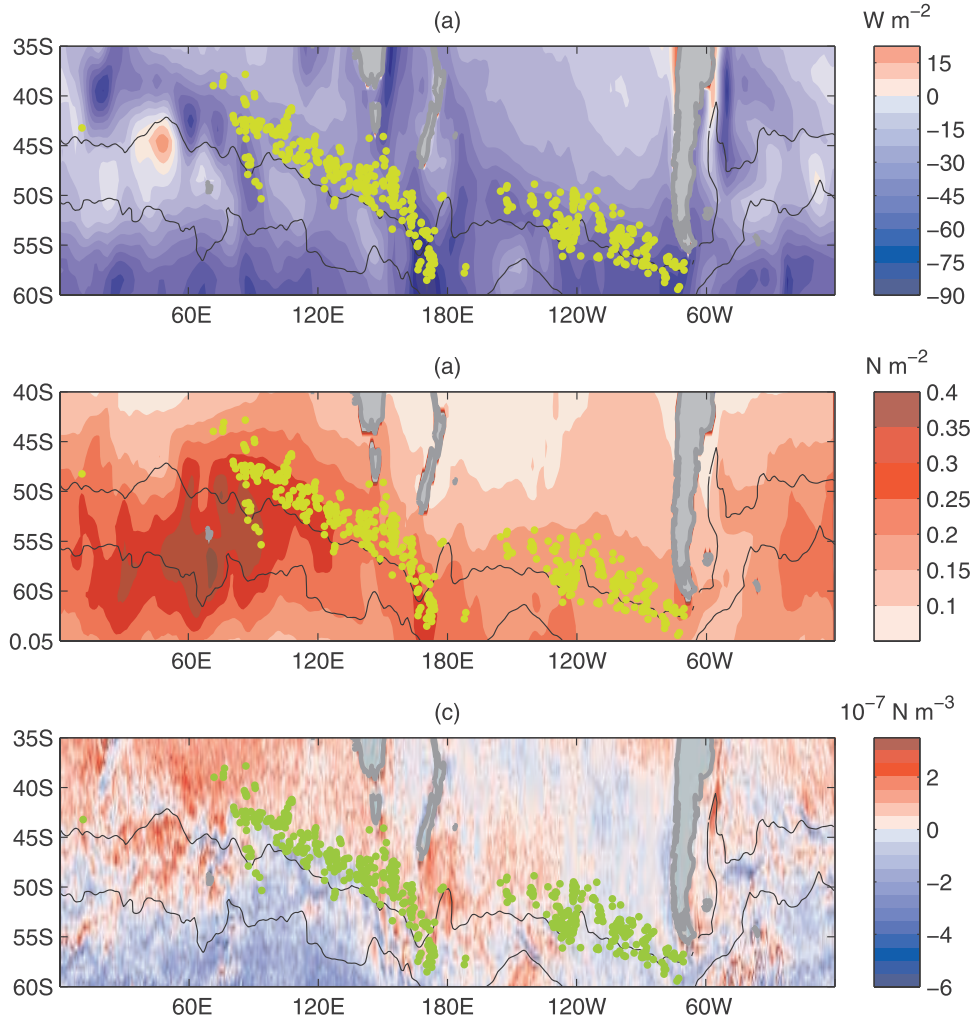


Figure 7. Four-year (1 June 1 2002 through 31 May 2006) average of (a) air-sea heat exchange (W m^{-2}), (b) zonal wind stress (N m^{-2}), and (c) wind stress curl (10^{-7} N m^{-3}) during the cooling season (April–September). Positive heat fluxes indicate heat input into the ocean from the atmosphere, and positive wind stress curl corresponds to downwelling. The green dots indicate the locations where MLD exceeds 400 m. Black curves as in Figure 1.

(Figure 5) which corresponds well to the density of the thickest Southeast Indian Ocean SAMW [Talley, 1999; Hanawa and Talley, 2001], consistent with Figure 6a which shows this density cluster only in the Southeast Indian Ocean.

[20] The formation region for SAMW in the Atlantic is limited [McCartney, 1982]. In the western Atlantic, SAMW and Subtropical Mode Water (STMW) are associated with the Brazil-Malvinas front, where STMW is found to the north of the front and SAMW on both sides of the front [Provost *et al.*, 1995]. The density definitions of SAMW from different studies [Provost *et al.*, 1999; Donners *et al.*, 2005] are not clearly distinguished from the density definition of STMW. Thus, it is difficult to separate SAMW from STMW in the Argo profiles that have MLDs exceeding 200 m. So, the properties of the Atlantic SAMW are not discussed here.

[21] The wintertime deep mixed layers and formation of the SAMW have been related to air-sea heat exchange and wind-forcing [e.g., McCartney, 1977]. A large heat loss from the ocean to the atmosphere during winter causes

vertical convection which results in a deep mixed layer. Strong wind mixing can also result in a deep mixed layer. In addition, the oceanic advection, transport convergence, and the initial stratification before the cooling season can also play a role in forming deep mixed layers. Here we examine their relationship using air-sea heat fluxes calculated from the National Center for Environmental Prediction/National Center for Atmospheric Research (NCEP/NCAR) Reanalysis fields [Kalnay *et al.*, 1996] using the state-of-the-art bulk flux algorithm version 3.0 developed from the Coupled Ocean-Atmosphere Response Experiment (COARE 3.0) [Fairall *et al.*, 2003]. Details of the calculation are given by Dong *et al.* [2007]. We also examine the relationship of the SAMW with wind stress and wind stress curl using wind stress fields from QuikSCAT scatterometry [Pegion *et al.*, 2000] and a blended wind stress curl product from QuikSCAT scatterometry and NCEP [Milliff *et al.*, 1999].

[22] The locations with deep mixed layers are well within the region of strong wintertime cooling just to the north of the ACC (Figure 7a), consistent with the idea that deep

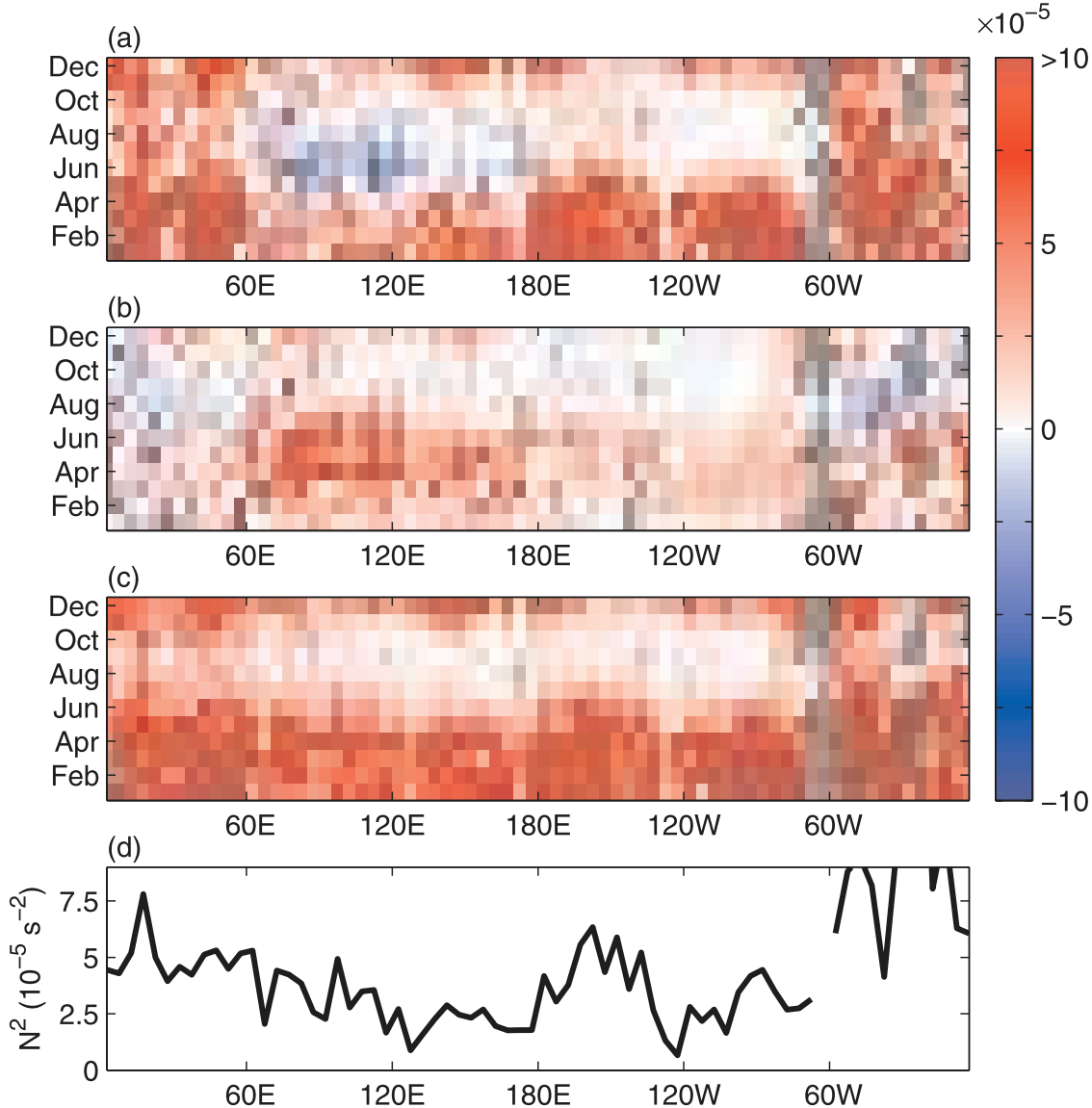


Figure 8. Vertical stratification of (a) temperature ($-g\alpha\partial T/\partial z$), (b) salinity ($g\beta\partial S/\partial z$), and (c) density ($g/\rho \partial \rho/\partial z$) averaged within 10 m below the mixed layer in a 5-degree band north of the ACC. Positive values (red) correspond to stable stratification. (d) The density stratification (the Brunt-Vaisala frequency squared) averaged from May to July. Units are 10^{-5} s^{-2} .

convection from wintertime cooling leads to the formation of mode water. The wind stress (Figure 7b) in the Indian Ocean is much stronger than that in the Pacific, which results in strong mixing, and hence a deep mixed layer. The strong wind also results in a strong horizontal Ekman advection in the Indian Ocean, which brings more cold water from the south to the mode water formation region, assisting the development of deep mixed layers. The deep mixed layers in the eastern Indian and western Pacific also correspond well to the location of the mean zero wind stress curl (Figure 7c), indicating that the mode water formation region coincides with the region of the strongest wind. Again, the strong mixing from wind may assist the formation of mode water. However, in the eastern Pacific the deep mixed layers are within regions where the wind stress curl is negative, corresponding to Ekman upwelling which may

play a role in weakening the vertical stratification. The heat loss to the atmosphere in the eastern Pacific (Figure 7a) is stronger than that in the Indian Ocean, suggesting that air-sea heat exchange may play a relatively larger role in mode water formation in the eastern Pacific.

[23] The difference between the eastern Pacific and eastern Indian is also evident in the stratification of temperature and salinity (Figures 8a and 8b) just below the mixed layer, here averaged within a 5° latitude band north of the ACC that corresponds to the region of SAMW formation and the deep mixed layers. Again, the SSH contour of -0.4 m from the monthly mean SSH maps is used to represent the seasonal variability of the northern boundary of the ACC. We also calculated the stratification using the mean Subantarctic Front locations from previous studies [Orsi *et al.*, 1995; Belkin and Gordon, 1996; Gille, 1999]. The results

are all similar to Figures 8a and 8b, suggesting that the stratification is not sensitive to our representation of the ACC. Both the Pacific and Indian oceans show a stable water column year round and a similar density stratification (Figure 8c). Temperature controls the density stratification in the Pacific. In contrast, in the Indian Ocean salinity stabilizes the water column, particularly during the cooling season when the Indian Ocean experiences temperature inversions (Figure 8a). The increase in density from salinity compensates the decrease in density from the temperature inversion at the base of the mixed layer (Figure 8b). This cold and fresh water in the Indian Ocean is potentially advected from the South owing to the strong wind, which may partially explain the weak heat loss to the atmosphere compared to the eastern Pacific. The differences in the temperature and salinity stratification and in wind-forcing between the eastern Pacific and eastern Indian Ocean suggest that the mode water formation in each region may be preconditioned by different processes. In the eastern Pacific, wind stress curl induced upwelling weakens the vertical stratification, which may play an important role in preconditioning for mode water formation. The strong cooling may also play a large role in forming deep mixed layer for temperature-stabilized water column. In contrast in the Indian Ocean, the strong wind mixing and northward Ekman advection of the cold and fresh Antarctic Surface Water and the advection of the warm and salty Agulhas Return water upstream may have a larger impact on the vertical stratification.

[24] As shown in Figures 6 and 7, only one Argo profile gives a MLD exceeding 400 m in the Atlantic Ocean, and no deep mixed layers are found between 180° and 200°E during our study period. The water column in these regions is strongly stabilized mainly by temperature (Figures 8a and 8c). The strong density stratification in the Atlantic and between 180° – 200°E is demonstrated more clearly in Figure 8d, which shows the density stratification averaged from May to July before the MLD reaches its maximum. This suggests that the strong stratification in these regions probably prevents deep convection from occurring.

4. Conclusion

[25] Argo float profiles of temperature, salinity and pressure are used to determine MLDs in the Southern Ocean (30°S – 65°S , 0°E – 360°E). Here the MLD is determined from individual profiles based on density ($\Delta\rho = 0.03 \text{ kg m}^{-3}$) and temperature ($|\Delta T| = 0.2^{\circ}\text{C}$) difference criteria. Salinity can play a strong role in the density stratification of the Southern Ocean. Nearly 24% of the total temperature profiles experience inversions. Temperature inversions are not limited to winter, but can occur in all seasons, and furthermore the temperature structure in the upper water column can vary depending on the season. The wintertime profiles are dominated by a cold layer in the upper ocean. During spring and summer, the upper part of the cold layer warms and caps the cold water below, and then the surface warm layer cools again in fall and winter. Salinity decreases with depth away from the ACC; in contrast in the vicinity of the ACC and to its south, and in the eastern Pacific salinity increases with depth. The dominant role of salinity in the stratification and the

temperature inversions suggest that the Southern Ocean MLDs are likely to pose different challenges than MLDs in regions that are strictly temperature stratified. This implies that when using a temperature difference criterion to determine MLD, it is important that *absolute* temperature differences ($|T_s - T_d|$) relative to the surface temperature are used to determine the true MLD.

[26] A monthly climatology (see auxiliary material for the quantitative data) is derived from individual MLDs using an objective mapping method. The spatial structure of the MLD is similar in each month, with deep mixed layers within and just north of the ACC in the eastern Pacific and Indian oceans. The MLD varies seasonally with the deepest mixed layers in August/September and the shallowest in January/February. The spatial distribution of the deep mixed layers is consistent with the formation region of SAMW. Examination of individual MLDs indicates that the deep mixed layers ($\text{MLD} \geq 400 \text{ m}$) from both the density and temperature criteria are concentrated in a narrow density band (26.57 – 27.04 kg m^{-3}) which is within the density range of SAMW. The narrowness of the density band is attributed to the compensation between decreasing temperature and salinity from the Indian Ocean to the eastern Pacific. The sea surface salinity for those deep mixed layers is slightly fresher than the salinity historically reported for the SAMW. The surface density increases and temperature decreases as the ACC shifts southward from the Indian Ocean to Drake Passage, which is consistent with the spatial variability of the SAMW properties [Hanawa and Talley, 2001].

[27] Deep mixed layers are well within the region of strong wintertime cooling, consistent with the idea that deep convection from wintertime cooling leads to the formation of mode water. However, the strong wind in the Indian Ocean and the colocation of the strong wind with the region of mode water formation suggest that the wind mixing and Ekman transport of cold water from the south may assist the formation of mode water. In contrast in the eastern Pacific, the formation of mode water is potentially preconditioned by the relative strong cooling and weak stratification from upwelling.

Appendix A

[28] The auxiliary material for this paper include four different mixed-layer depth climatologies. As discussed in the text, one is based on a potential density difference of $\Delta\rho > 0.03 \text{ kg m}^{-3}$, a second on a potential temperature difference of $|\Delta T| > 0.2^{\circ}\text{C}$, a third on the potential density-based hybrid method of Holte and Talley (submitted manuscript, 2008), and the fourth on Holte and Talley's (submitted manuscript, 2008) temperature method. Monthly values are objectively mapped to $1^{\circ} \times 1^{\circ}$ resolution, and formal objective mapping errors are reported.

[29] As noted in the text, the temperature difference between water in the mixed layer and water entrained into the mixed layer along its base (δT) varies spatially and temporally. Objectively mapped monthly climatologies for these values corresponding to the MLDs based on the temperature and density difference criteria are also reported, along with error estimates. Note that for each Argo profile values of δT based on the potential temperature difference

criterion are formally either $+0.2^{\circ}\text{C}$ or -0.2°C , though the mapping procedure averages these individual values to give a range of δT .

[30] **Acknowledgments.** This study is supported by NASA grant EOS/03-0602-0117 and by NASA/JPL contract 1224031. The Argo float profiles are managed by the Global Ocean Data Assimilation Experiment (GODAE) and are available from <http://www.usgodae.org/ftp/outgoing/argo/dac/>.

References

- Alexander, M. A., and C. Deser (1995), A mechanism for the recurrence of wintertime Midlatitude SST anomalies, *J. Phys. Oceanogr.*, **25**, 122–137, doi:10.1175/1520-0485(1995)025<0122:AMFTRO>2.0.CO;2.
- Banks, H. T., R. A. Wood, J. M. Gregory, T. C. Johns, and G. S. Jones (2000), Are observed decadal changes in intermediate water masses a signature of anthropogenic climate change?, *Geophys. Res. Lett.*, **27**, 2961–2964, doi:10.1029/2000GL011601.
- Banks, H. T., R. A. Wood, and J. M. Gregory (2002), Changes to Indian Ocean Subantarctic Mode Water in a coupled climate model as CO₂ forcing increases, *J. Phys. Oceanogr.*, **32**, 2816–2827, doi:10.1175/1520-0485(2002)032<2816:CTIOSM>2.0.CO;2.
- Belkin, I. M., and A. L. Gordon (1996), Southern Ocean fronts from the Greenwich meridian to Tasmania, *J. Geophys. Res.*, **101**, 3675–3696, doi:10.1029/95JC02750.
- Bhatt, U. S., M. A. Alexander, and D. S. Battisti (1998), Atmosphere-ocean interaction in the North Atlantic: Near-surface climate variability, *J. Clim.*, **11**, 1615–1632, doi:10.1175/1520-0442(1998)011<1615:AOIITN>2.0.CO;2.
- Brainerd, K. E., and M. C. Gregg (1995), Surface mixed and mixing layer depths, *Deep Sea Res., Part A*, **42**, 1521–1543.
- Bretherton, F. P., R. E. Davis, and C. B. Fandry (1976), A technique for objective analysis and design of oceanographic experiments applied to MODE-73, *Deep Sea Res.*, **23**, 559–582.
- de Boyer Montegut, C., G. Madec, A. S. Fischer, A. Lazar, and D. Iudicone (2004), Mixed layer depth over the global ocean: An examination of profile data and a profile-based climatology, *J. Geophys. Res.*, **109**, C12003, doi:10.1029/2004JC002378.
- Deser, C. M. A. A., and M. S. Timlin (2003), Understanding the persistence of the sea surface temperature anomalies in the mid-latitudes, *J. Clim.*, **16**, 57–72, doi:10.1175/1520-0442(2003)016<0057:UTPOSS>2.0.CO;2.
- Dommelier, D., and M. Latif (2002), Analysis of observed and simulated SST spectra in the midlatitudes, *Clim. Dyn.*, **19**, 277–288, doi:10.1007/s00382-002-0229-9.
- Dong, S., and K. A. Kelly (2004), Heat budget in the Gulf Stream region: The importance of heat storage and advection, *J. Phys. Oceanogr.*, **34**, 1214–1231, doi:10.1175/1520-0485(2004)034<1214:HBITGS>2.0.CO;2.
- Dong, S., J. Sprintall, and S. T. Gille (2006), Location of the polar front from AMSR-E satellite sea surface temperature measurements, *J. Phys. Oceanogr.*, **36**, 2075–2089, doi:10.1175/JPO2973.1.
- Dong, S., S. T. Gille, and J. Sprintall (2007), An assessment of the Southern Ocean mixed-layer heat budget, *J. Clim.*, **20**, 4425–4442, doi:10.1175/JCLI4259.1.
- Donners, J., S. S. Drijfhout, and W. Hazeleger (2005), Water mass transformation and subduction in the South Atlantic, *J. Phys. Oceanogr.*, **35**, 1841–1860, doi:10.1175/JPO2782.1.
- Ducet, N., P.-Y. Le Traon, and G. Reverdin (2000), Global high-resolution mapping of ocean circulation from TOPEX/POSEIDON and ERS-1 and -2, *J. Geophys. Res.*, **105**, 19,477–19,498, doi:10.1029/2000JC900063.
- Fairall, C. W., E. F. Bradley, J. E. Hare, A. A. Grachev, and J. B. Edson (2003), Bulk parameterization of air-sea fluxes: Updates and verification for the COARE algorithm, *J. Clim.*, **16**, 571–591, doi:10.1175/1520-0442(2003)016<0571:BPOASF>2.0.CO;2.
- Gille, S. T. (1999), Mass, heat, and salt transport in the southeastern Pacific: A circumpolar current inverse model, *J. Geophys. Res.*, **104**, 5191–5210, doi:10.1029/1998JC900106.
- Gould, J., and the Argo steering team (2004), Argo profiling floats bring new era of in situ ocean observations, *Eos Trans. AGU*, **85**(19), 185, doi:10.1029/2004EO190002.
- Hanawa, K., and L. D. Talley (2001), Mode waters, in *Ocean Circulation and Climate*, edited by G. Siedler and J. Church, pp. 373–386, Academic Press, San Diego, Calif.
- Kalnay, E., et al. (1996), The NCEP/NCAR 40-year reanalysis project, *Bull. Am. Meteorol. Soc.*, **77**, 437–471, doi:10.1175/1520-0477(1996)077<0437:TNYRP>2.0.CO;2.
- Lorbacher, K., D. Dommelier, P. P. Niiler, and A. Köhl (2006), Ocean mixed layer depth: A subsurface proxy of ocean-atmosphere variability, *J. Geophys. Res.*, **111**, C07010, doi:10.1029/2003JC002157.
- Maximenko, N. A., and P. P. Niiler (2005), Hybrid decade-mean global sea level with mesoscale resolution, in *Recent Advances in Marine Science and Technology, 2004*, edited by N. Saxena, pp. 55–59, PACON Int., Honolulu, Hawaii.
- McCartney, M. S. (1977), Subantarctic mode water, *Deep Sea Res.*, **24**, 103–119.
- McCartney, M. S. (1982), The subtropical recirculation of mode waters, *J. Mar. Res.*, **40**(suppl.), 427–464.
- Milliff, R. F., W. G. Large, J. Morzel, G. Danabasoglu, and T. M. Chin (1999), Ocean general circulation model sensitivity to forcing from scatterometer winds, *J. Geophys. Res.*, **104**, 11,337–11,358, doi:10.1029/1998JC900045.
- Monterey, G. I., and S. Levitus (1997), Climatological cycle of mixed layer depth in the world ocean, report, 5 pp., NOAA, Silver Spring, Md.
- Moore, J. K., M. R. Abbott, and J. G. Richman (1999), Location and dynamics of the Antarctic Polar Front from satellite sea surface temperature data, *J. Geophys. Res.*, **104**, 3059–3073, doi:10.1029/1998JC900032.
- Orsi, A. H., T. Whitworth III, and W. D. Nowlin Jr. (1995), On the meridional extent and fronts of the Antarctic Circumpolar Current, *Deep Sea Res., Part II*, **42**, 641–673, doi:10.1016/0967-0637(95)00021-W.
- Pegion, P. J., M. A. Bourassa, D. M. Legler, and J. J. O'Brien (2000), Objectively derived daily “winds” from satellite scatterometer data, *Mon. Weather Rev.*, **128**, 3150–3168, doi:10.1175/1520-0493(2000)128<3150:ODDWFS>2.0.CO;2.
- Provost, C., S. Gana, V. Garçon, K. Maamaatauaiahutapu, and M. England (1995), Hydrographic conditions in the Brazil-Malvinas Confluence during austral summer 1990, *J. Geophys. Res.*, **100**, 10,655–10,678, doi:10.1029/94JC02864.
- Provost, C., C. Escoffier, K. Maamaatauaiahutapu, A. Kartavtseff, and V. Garçon (1999), Subtropical mode waters in the South Atlantic Ocean, *J. Geophys. Res.*, **104**, 21,033–21,049, doi:10.1029/1999JC900049.
- Qiu, B. (2000), Interannual variability of the Kuroshio Extension system and its impact on the wintertime SST field, *J. Phys. Oceanogr.*, **30**, 1486–1502, doi:10.1175/1520-0485(2000)030<1486:IVOTKE>2.0.CO;2.
- Roemmich, D. (1983), Optimal estimation of hydrographic station data and derived fields, *J. Phys. Oceanogr.*, **13**, 1544–1549, doi:10.1175/1520-0485(1983)013<1544:OEHOHS>2.0.CO;2.
- Sallee, J., N. Wienders, K. Speer, and R. Morrow (2006), Formation of subantarctic mode water in the southeastern Indian Ocean, *Ocean Dyn.*, **56**, 525–542, doi:10.1007/s10236-005-0054-x.
- Schneider, W., and L. Bravo (2006), Argo profiling floats document Subantarctic Mode Water formation west of Drake Passage, *Geophys. Res. Lett.*, **33**, L16609, doi:10.1029/2006GL026463.
- Sloyan, B. M., and S. R. Rintoul (2001), The Southern Ocean limb of the global deep overturning circulation, *J. Phys. Oceanogr.*, **31**, 143–173, doi:10.1175/1520-0485(2001)031<0143:TSOLOT>2.0.CO;2.
- Talley, L. D. (1999), Some aspects of ocean heat transport by the shallow, intermediate and deep overturning circulations, in *Mechanisms of Global Climate Change at Millennial Time Scales*, *Geophys. Monogr. Ser.*, vol. 112, edited by P. Clark, R. Webb, and L. Keigwin, PP. 1–22, AGU, Washington, D. C.
- Thomson, R. E., and I. V. Fine (2003), Estimating mixed layer depth from oceanic profile data, *J. Atmos. Oceanic Technol.*, **20**, 319–329, doi:10.1175/1520-0426(2003)020<0319:EMLDFO>2.0.CO;2.
- Vivier, F., K. A. Kelly, and L. Thompson (2002), Heat budget in the Kuroshio Extension region: 1993–1999, *J. Phys. Oceanogr.*, **32**, 3436–3454, doi:10.1175/1520-0485(2002)032<3436:HBITKE>2.0.CO;2.
- Weller, R. A., and A. J. Plueddemann (1996), Observations of the vertical structure of the oceanic boundary layer, *J. Geophys. Res.*, **101**, 8789–8806, doi:10.1029/96JC00206.
- Wijesekera, R. W., and M. C. Gregg (1996), Surface layer response to weak winds, westerly bursts, and rain squalls in western Pacific warm pool, *J. Geophys. Res.*, **101**, 977–997, doi:10.1029/95JC02553.
- Wong, A. P. S., N. L. Bindoff, and J. A. Church (1999), Large-scale freshening of intermediate waters in the Pacific and Indian oceans, *Nature*, **400**, 440–443, doi:10.1038/22733.

S. Dong, CIMAS/RSMAS, University of Miami, 4600 Rickenbacker Causeway, Miami, FL 33149, USA. (shenfu.dong@noaa.gov)

S. T. Gille, J. Sprintall, and L. Talley, Scripps Institution of Oceanography, University of California, San Diego, 9500 Gilman Drive, Mail Code 0230, La Jolla, CA 92093-0230, USA.